Monthly Notices
of the
ROYAL ASTRONOMICAL SOCIETY

MNRAS 450, 4475–4485 (2015) doi:10.1093/mnras/stv884

Deriving the orbital properties of pulsators in binary systems through their light arrival time delays

Simon J. Murphy[1,2]★ and Hiromoto Shibahashi[3]★

[1]Sydney Institute for Astronomy, School of Physics, The University of Sydney, NSW 2006, Australia
[2]Stellar Astrophysics Centre, Department of Physics and Astronomy, Aarhus University, DK-8000 Aarhus C, Denmark
[3]Department of Astronomy, The University of Tokyo, Tokyo 113-0033, Japan

Accepted 2015 April 18. Received 2015 April 16; in original form 2015 February 10

ABSTRACT

We present the latest developments to the phase modulation method for finding binaries among pulsating stars. We demonstrate how the orbital elements of a pulsating binary star can be obtained analytically, that is, without converting time delays to radial velocities by numerical differentiation. Using the time delays directly offers greater precision, and allows the parameters of much smaller orbits to be derived. The method is applied to KIC 9651065, KIC 10990452 and KIC 8264492, and a set of the orbital parameters is obtained for each system. Radial velocity curves for these stars are deduced from the orbital elements thus obtained.

Key words: asteroseismology – stars: individual: KIC 8264492 – stars: individual: KIC 9651065 – stars: individual: KIC 10990452 – stars: oscillations.

1 INTRODUCTION

Radial velocities are fundamental data of astronomy. Not only in a cosmological context, where the recessional and rotational velocities of galaxies are of interest, but also in stellar astrophysics. A time series of radial velocity (RV) data for a binary system allows the orbital parameters of that system to be calculated. However, the importance of such data, which are meticulous and time-consuming to obtain, creates a large gap between demand and supply.

In the first paper of this series (Murphy et al. 2014), we described a method of calculating RV curves using the pulsation frequencies of stars as a 'clock'. For a star in a binary system, the orbital motion leads to a periodic variation in the path length travelled by light emitted from the star and arriving at Earth. Hence, if the star is pulsating, the observed phase of the pulsation varies over the orbit. We called the method 'PM' for phase modulation. Equivalently, one can study orbital variations in the frequency domain, which lead to frequency modulation (FM; Shibahashi & Kurtz 2012). Similar methods of using photometry to find binary stars have been developed recently by Koen (2014) and Balona (2014), though the FM and PM methods are the first to provide a full orbital solution from photometry alone. Indeed, the application of PM to coherent pulsators will produce RV curves for hundreds of *Kepler* stars without the need for ground-based spectroscopy, alleviating the bottleneck.

The crux of the PM method is the conversion of pulsational phase modulation into light arrival time delays (TDs), for several pulsation frequencies in the same star. While the phase modulation is a frequency-dependent quantity, the TD depends on the orbital properties, only. Hence for all pulsation frequencies, the response of the TDs to the binary orbit is the same, which distinguishes this modulation from other astrophysical sources, such as mode interaction (see e.g. Buchler, Goupil & Hansen 1997).

Previously, our approach used numerical differentiation of the TDs to produce an RV curve, from which the final orbital solution was determined. The RV curves thus obtained were sometimes unrealistic due to scatter in the TDs. Recognizing numerical differentiation as the weakness of the method, we have now developed a method of deriving the orbital properties from the TDs directly, without the need to convert TDs into RVs. It is this method that we describe in this paper. The RV curve is produced afterwards, from the orbital properties, and is no longer a necessary step in the analysis.

2 TD ANALYSIS: METHODOLOGY AND EXAMPLE 1: KIC 9651065

Let us divide the light curve into short segments and measure the phase of pulsation in each segment. This provides us with TDs, $\tau_{\rm obs}(t_n)$, as observational data, where t_n ($n = 1, 2, \ldots$) denotes the time series at which observations are available. Fig. 1 shows an example TD diagram (for the case of KIC 9651065), where TDs vary periodically with the binary orbital period. The TD difference between the maximum and the minimum gives the projected size of the orbit in units of light-seconds. Deviation from a sinusoid indicates that the orbit is eccentric. The TD curve is given a zero-point by subtracting the mean of the TDs from each observation. The pulsating star is furthest from us when the TD curve reaches its maxima, while the star is nearest to us at the minima. The sharp

★ E-mail: murphy@physics.usyd.edu.au (SJM); shibahashi@astron.s.u-tokyo.ac.jp (HS)

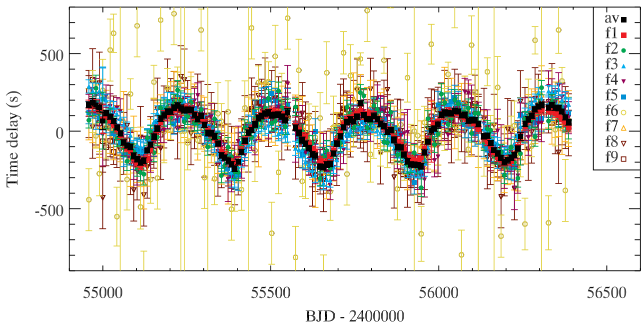

Figure 1. An example of TD curve (KIC 9651065) using nine different pulsation modes, including one in the super-Nyquist frequency range (Murphy, Shibahashi & Kurtz 2013). The weighted average is shown as filled black squares.

minima and blunt maxima in Fig. 1 indicate that periapsis is at the near side of the orbit. The asymmetry of the TD curve, showing fast rise and slow fall, reveals that the star passes the periapsis after reaching the nearest point to us. In this way, TD curves provide us with information about the orbit.

Theoretically, TD is expressed as a function $\tau_{\rm th}(t)$ of time t and the orbital elements: (i) the orbital period $P_{\rm orb}$, or equivalently, the orbital frequency $\nu_{\rm orb} := 1/P_{\rm orb}$, or the orbital angular frequency $\Omega := 2\pi\nu_{\rm orb}$, (ii) the projected semimajor axis $a_1 \sin i$, (iii) the eccentricity e, (iv) the angle between the nodal point and the periapsis ϖ,[1] and (v) the time of periapsis passage $t_{\rm p}$. Hence, these orbital elements can be determined from the observed TD as a set of parameters giving the best-fitting $\tau_{\rm th}(t)$.

2.1 Least-squares method

The best-fitting parameters can be determined by searching for the minimum of the sum of square residuals

$$\chi^2(\boldsymbol{x}, \lambda) := \sum_n \frac{1}{\sigma_n^2}\left[\tau_{\rm th}(t_n, \boldsymbol{x}) - \tau_{\rm obs}(t_n) - \lambda\right]^2, \tag{1}$$

where σ_n denotes the observational error in measurement of $\tau_{\rm obs}(t_n)$. Here the parameter dependence of $\tau_{\rm th}(t)$ is explicitly expressed with the second argument $\boldsymbol{x}$, which denotes the orbital elements as a vector, and a parameter λ is introduced to compensate for the freedom of $\tau_{\rm obs}(t_n) = 0$ (i.e. the arbitrary vertical zero-point). Hence the parameters $\boldsymbol{x}$ and λ satisfying $\partial\chi^2/\partial\boldsymbol{x} = 0$ and $\partial\chi^2/\partial\lambda = 0$ are to be found, that is,

$$\sum_n \frac{1}{\sigma_n^2}\left[\tau_{\rm th}(t_n, \boldsymbol{x}) - \tau_{\rm obs}(t_n) - \lambda\right]\frac{\partial\tau_{\rm th}(t_n, \boldsymbol{x})}{\partial\boldsymbol{x}} = 0 \tag{2}$$

and

$$\lambda = \left(\sum_n \frac{1}{\sigma_n^2}\right)^{-1} \sum_n \frac{1}{\sigma_n^2}\left[\tau_{\rm th}(t_n, \boldsymbol{x}) - \tau_{\rm obs}(t_n)\right]. \tag{3}$$

2.2 TDs as a function of orbital elements

In order to solve equation (2), we have to derive the explicit dependence of $\tau_{\rm th}$ on the orbital elements. The readers may consult with the literature such as Freire, Kramer & Lyne (2001, Erratum: Freire, Kramer & Lyne 2009). We derive $\tau_{\rm th}$ following Shibahashi & Kurtz (2012) in this subsection. See also Shibahashi, Kurtz & Murphy (2015).

Let us define a plane that is tangential to the celestial sphere on which the barycentre of the binary is located, and let the z-axis that is perpendicular to this plane and passing through the barycentre of the binary be along the line-of-sight towards us (see Fig. 2). The orbital plane of the binary motion is assumed to be inclined to the celestial sphere by the angle i, which ranges from 0 to π. The orbital motion of the star is in the direction of *increasing* position angle, if $0 \le i < \pi/2$, and in the direction of *decreasing* position angle, if $\pi/2 < i \le \pi$.

Let r be the distance between the centre of gravity and the star when its true anomaly is f. The difference in the light arrival time, τ, compared to the case of a signal arriving from the barycentre of the binary system is given by

$$\tau = -r\sin(f + \varpi)\sin i/c, \tag{4}$$

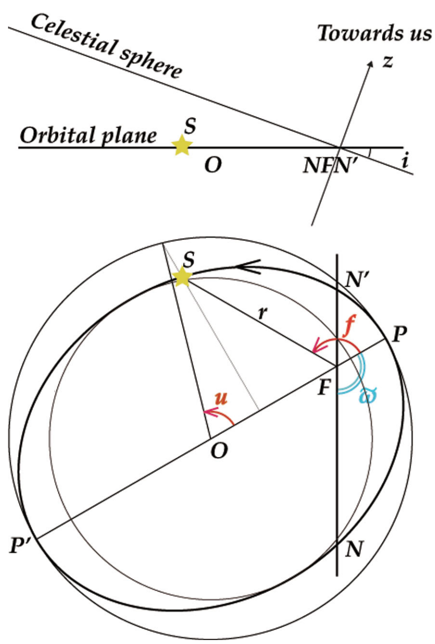

Figure 2. Top: schematic side view of the orbital plane, seen from a faraway point along the intersection of the orbital plane and the celestial sphere, NFN', where the points N and N' are the nodal points, respectively, and the point F is the centre of gravity of the binary system; that is, a focus of the orbital ellipses. The orbital plane is inclined to the celestial sphere by the angle i, which ranges from 0 to π. In the case of $0 \le i < \pi/2$, the orbital motion is in the direction of increasing position angle of the star, while in the case of $\pi/2 < i \le \pi$, the motion is the opposite. The z-axis is the line-of-sight towards us, and $z = 0$ is the plane tangential to the celestial sphere. Bottom: schematic top view of the orbital plane along the normal to that plane. The periapsis of the elliptical orbit is P. The angle measured from the nodal point N, where the motion of the star is directed towards us, to the periapsis in the direction of the orbital motion of the star is denoted as ϖ. The star is located, at this moment, at S on the orbital ellipse, for which the focus is F. The semimajor axis is a and the eccentricity is e. Then $\overline{\rm OF}$ is ae. The distance between the focus, F, and the star, S, is r. The angle PFS is 'the true anomaly', f, measured from the periapsis to the star at the moment in the direction of the orbital motion of the star. 'The eccentric anomaly', u, also measured in the direction of the orbital motion of the star, is defined through the circumscribed circle that is concentric with the orbital ellipse. Figure and caption from Shibahashi et al. (2015), this volume.

[1] We have chosen to represent this angle with ϖ, rather than with ω, because of the common use of ω to represent angular oscillation frequencies in asteroseismology.

where ϖ is the angle from the nodal point to the periapsis, i is the inclination angle and c is the speed of the light (see Fig. 2). Note that τ is defined so that it is negative when the star is nearer to us than the barycentre.[2] The distance r is expressed with the help of a combination of the semimajor axis a_1, the eccentricity e, and the true anomaly f:

$$r = \frac{a_1(1-e^2)}{1+e\cos f}. \tag{5}$$

Hence,

$$\tau(t, \boldsymbol{x}) = -\frac{a_1 \sin i}{c}(1-e^2)\frac{\sin f \cos\varpi + \cos f \sin\varpi}{1+e\cos f}. \tag{6}$$

The trigonometric functions of f are expressed in terms of a series expansion of trigonometric functions of the time after the star passed the periapsis with Bessel coefficients:

$$\cos f = -e + \frac{2(1-e^2)}{e}\sum_{n=1}^{\infty} J_n(ne)\cos n\Omega(t-t_\mathrm{p}), \tag{7}$$

$$\sin f = 2\sqrt{1-e^2}\sum_{n=1}^{\infty} J_n{}'(ne)\sin n\Omega(t-t_\mathrm{p}), \tag{8}$$

where $J_n(x)$ denotes the Bessel function of the first kind of integer order n and $J_n{}'(x) := \mathrm{d}J_n(x)/\mathrm{d}x$. Equation (6) with the help of equations (7) and (8) gives the TD τ_th at time t_n for a given set of $\boldsymbol{x} = (\Omega, a_1 \sin i/c, e, \varpi, t_\mathrm{p})$.

2.3 Simultaneous equations

Equation (2) forms a set of simultaneous equations for the unknown $\boldsymbol{x}$ with the help of equation (6). Let us rewrite symbolically equation (2) as

$$\boldsymbol{y}(\boldsymbol{x}) := \sum_n \alpha_n(\boldsymbol{x})\frac{\partial \tau_\mathrm{th}(t_n, \boldsymbol{x})}{\partial \boldsymbol{x}} = 0, \tag{9}$$

where

$$\alpha_n := \frac{1}{\sigma_n^2}\left[\tau_\mathrm{th}(t_n, \boldsymbol{x}) - \tau_\mathrm{obs}(t_n) - \lambda\right]. \tag{10}$$

This simultaneous equation can be solved by iteration, once we have a good initial guess $\boldsymbol{x}^{(0)}$:

$$\boldsymbol{y}\left(\boldsymbol{x}^{(0)}\right) + \left(\frac{\partial \boldsymbol{y}}{\partial \boldsymbol{x}^{(0)}}\right)\delta\boldsymbol{x} = 0, \tag{11}$$

then

$$\delta\boldsymbol{x} = -\left(\frac{\partial \boldsymbol{x}}{\partial \boldsymbol{x}^{(0)}}\right)^{-1}\boldsymbol{y}\left(\boldsymbol{x}^{(0)}\right). \tag{12}$$

Hence we need a means to obtain a good initial guess $\boldsymbol{x}^{(0)}$.

2.4 Initial guesses

2.4.1 Input parameters: observational constraints

An observed TD curve shows, of course, a periodic variation with the angular frequency Ω. By carrying out the Fourier transform of the observed TD curve, we determine Ω accurately. The presence of harmonics (2Ω, 3Ω, ...) indicates that the TDs deviate from a pure sinusoid. Hence, the angular frequency Ω is fairly accurately obtained from the Fourier transform of the observed TD curve (Fig. 3). Let A_1 and A_2 be the amplitudes in the frequency spectrum corresponding to the angular frequencies Ω and 2Ω, respectively. They are also accurately determined, by a simultaneous non-linear least-squares fit to the TD curve. By folding the observational data $\{\tau_\mathrm{obs}(t_n)\}$ with the period $2\pi/\Omega$, we get the TD as a function of orbital phase, $\phi_n := \Omega(t_n - t_0)/(2\pi)$, where t_0 is the time of the first data point. We then know the orbital phases at which τ_obs reaches its maximum and minimum. In the case of KIC 9651065, shown in Fig. 1, the frequency spectrum is shown in Fig. 3, and the obtained quantities are summarized in Table 1. They are used as input parameters from which initial guesses for the orbital parameters are deduced.

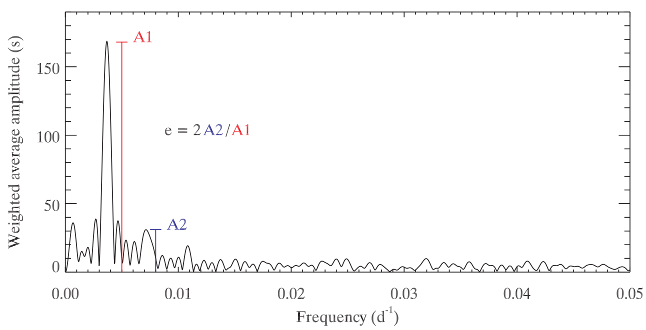

Figure 3. Fourier transform of the TD curve of KIC 9651065 shown in Fig. 1. After identification of A1 and A2 in the Fourier transform, their exact values and uncertainties are determined by a non-linear least-squares fit to the TD curve.

Table 1. Observational constraints for KIC 9651065.

Quantity	Value	Units
τ_max	136 ± 27	s
τ_min	-211 ± 42	s
ν_orb	$0.003\,685 \pm 0.000\,011$	d^{-1}
A_1	167.1 ± 3.06	s
A_2	35.7 ± 3.06	s
$\phi(\tau_\mathrm{max})$	0.54 ± 0.02	
$\phi(\tau_\mathrm{min})$	0.08 ± 0.02	

[2] That convention is established as follows. When the star lies beyond the barycentre, the light arrives later than if the star were at the barycentre: it is delayed. When the star is nearer than the barycentre, the TD is negative. A negative delay indicates an early arrival time. Since the observed luminosity, L, varies as

$$L \sim \cos\omega(t - d/c),$$

where d is the path length travelled by the light on its way to Earth, then the phase change, $\Delta\phi$, of the stellar oscillations is negative when the TD is increasing. That is,

$$\tau \propto -\Delta\phi.$$

The convention we hereby establish differs from that in PM I (Murphy et al. 2014, equation 3), where the minus sign was not included. We therefore had to introduce a minus sign into equations (6) and (7), there, in order to follow the convention that RV is positive when the object recedes from us. Hence, while the RV curves in that paper have the correct orientation, the TD diagrams there are upside-down. Our convention here fixes this.

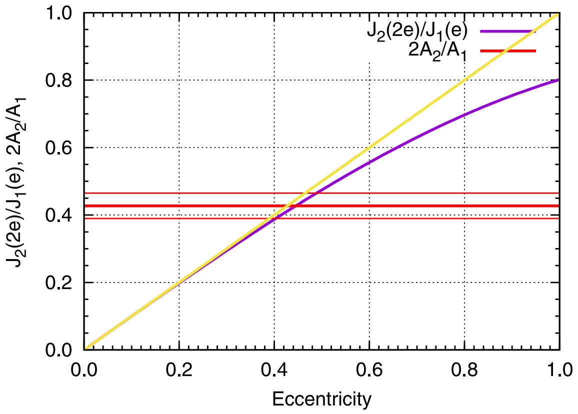

Figure 4. The amplitude ratio between the two components A_1 and A_2 of KIC 9651065 provides us with an initial guess of e. The thick horizontal red line is the measured $2A_2/A_1$, and the thin lines above and below it are the uncertainties.

2.4.2 Initial guess for e

The amplitude ratio between the two components A_1 and A_2 provides us with an initial guess of e (Shibahashi & Kurtz 2012; Murphy et al. 2014):

$$\frac{J_2(2e^{(0)})}{J_1(e^{(0)})} = \frac{2A_2}{A_1}, \tag{13}$$

where $J_1(x)$ and $J_2(x)$ denote the first kind of Bessel function, of the order of 1 and 2, respectively. This approximation is justified, as the ϖ dependence on the amplitude ratio is weak. In fact, this approximation is good for a wide range of ϖ. Even in the case of $e \simeq 1$, the approximation gives $e^{(0)} = 0.80$ (see Fig. 4), from which the correct value of e is recoverable. In the case of $e \ll 1$, the LHS of the above equation is further reduced to $\sim e$ (Murphy et al. 2014).

2.4.3 Initial guess for t_p

The largest and the smallest values of $\tau_{\rm obs}$ are well defined and easily identified, as are the epochs of these extrema. Therefore, the extrema and their epochs are useful for providing initial guesses for the remaining orbital elements.

First, let us see when these extrema occur. With the help of the known laws of motion in an ellipse (Brouwer & Clemence 1961),

$$r\frac{{\rm d}f}{{\rm d}t} = \frac{a_1\Omega(1+e\cos f)}{\sqrt{1-e^2}} \tag{14}$$

and

$$\frac{{\rm d}r}{{\rm d}t} = \frac{a_1\Omega e \sin f}{\sqrt{1-e^2}}, \tag{15}$$

where Ω denotes the orbital angular frequency, the time variation of τ shown in equation (4) is given by

$$\frac{{\rm d}\tau}{{\rm d}t} = -\frac{1}{c}\frac{\Omega a_1 \sin i}{\sqrt{1-e^2}}\left[\cos(f+\varpi)+e\cos\varpi\right]. \tag{16}$$

Hence, when τ reaches the extrema

$$\cos(f+\varpi) = -e\cos\varpi, \tag{17}$$

therefore

$$\sin(f+\varpi) = \pm\sqrt{1-e^2\cos^2\varpi}. \tag{18}$$

Since $c\,{\rm d}\tau/{\rm d}t = v_{\rm rad}$, the extrema of τ correspond to the epochs of $v_{\rm rad} = 0$. Geometrically, in Fig. 2, the extrema correspond to the tangential points of the ellipse to lines parallel to NN'. Note that the nearer side corresponds to negative TD while the farther side corresponds to positive TD. Hereafter, the orbital elements corresponding to the extremum of the nearer side are written with a subscript 'Near', and those of the farther side are distinguished with a subscript 'Far'. These two points are rotationally symmetric with respect to the centre of the ellipse, O. Hence the eccentric anomalies of these two points, $u_{\rm Near}$ and $u_{\rm Far}$, are different from each other by π radians:

$$u_{\rm Far} - u_{\rm Near} = \pi. \tag{19}$$

The eccentric anomaly u is written with Ω, e and t_p as

$$u = \Omega(t-t_{\rm p}) + 2\sum_{n=1}^{\infty}\frac{1}{n}J_n(ne)\sin n\Omega(t-t_{\rm p}). \tag{20}$$

Since the initial guesses for Ω and e are already available, the eccentric anomaly u in equation (20) is regarded as a function of t with a free parameter t_p. The epochs of the extrema of $\tau_{\rm obs}$, noted as $t_{\rm Near}$ and $t_{\rm Far}$, respectively, are observationally determined. Then, by substituting $t_{\rm Near}$ and $t_{\rm Far}$ into equation (20) and with a constraint given by equation (19),

$$\Omega(t_{\rm Far}-t_{\rm Near}) + 2\sum_{n=1}^{\infty}\frac{1}{n}J_n(ne) \times\left\{\sin n\Omega(t_{\rm Far}-t_{\rm p}) - \sin n\Omega(t_{\rm Near}-t_{\rm p})\right\} - \pi = 0. \tag{21}$$

This equation should be regarded as an equation with an unknown t_p. To get a good initial guess for $t_{\rm p}^{(0)}$, we define

$$\phi_{\rm p} := \frac{\Omega}{2\pi}(t_{\rm p}-t_0) \tag{22}$$

and

$$\Psi(\phi_{\rm p}) := 2\pi(\phi_{\rm Far}-\phi_{\rm Near}) + 2\sum_{n=1}^{\infty}\frac{1}{n}J_n(ne) \times\left\{\sin 2\pi n(\phi_{\rm Far}-\phi_{\rm p}) - \sin 2\pi n(\phi_{\rm Near}-\phi_{\rm p})\right\} - \pi. \tag{23}$$

We search for zero-points of $\Psi(\phi_{\rm p})$ for a given set of $(\phi_{\rm Near}, \phi_{\rm Far})$ and $e = e^{(0)}$, where $\phi_{\rm Far}$ and $\phi_{\rm Near}$ are the orbital phases corresponding to $\tau_{\rm max}$ and $\tau_{\rm min}$, respectively, that are already measured.

As in the case shown in Fig. 5, there are two roots satisfying

$$\Psi\left(\phi_{\rm p}^{(0)}\right) = 0, \tag{24}$$

one corresponding to the case (A) that the pulsating star in question passes the periapsis soon after the nearest point to us, and the other corresponding to the case (B) that the star passes the apoapsis just before the nearest point to us. It is expected then that the sum of ϖ derived from these two solutions is 2π, that is, these two solutions are explementary angles.

2.4.4 Initial guess for ϖ

Once ϕ_p is determined, equations (7) and (8) give the true anomaly at the nearest point, $f_{\rm Near}$;

$$\cos f_{\rm Near}^{(0)} = -e + \frac{2(1-e^2)}{e}\sum_{n=1}^{\infty}J_n(ne)\cos 2\pi n(\phi_{\rm Near}-\phi_{\rm p}), \tag{25}$$

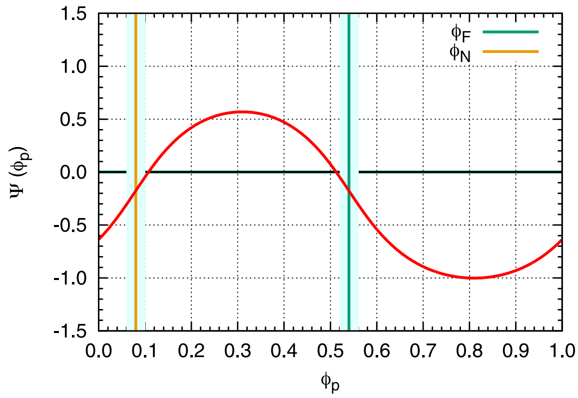

Figure 5. $\Psi(\phi_{\rm p})$ (red curve) for KIC 9651065. The zero crossings each give an initial estimate for $\phi_{\rm p}^{(0)}$; $\Psi(\phi_{\rm p}^{(0)}) = 0$. Vertical lines at '$\phi_{\rm F}$' and '$\phi_{\rm N}$' show the orbital phases of the furthest and the nearest points, corresponding to the maximum and the minimum of the TD, respectively. The light cyan bands show the uncertainty ranges of $\phi_{\rm F}$ and $\phi_{\rm N}$.

$$\sin f_{\rm Near}^{(0)} = 2\sqrt{1-e^2}\sum_{n=1}^{\infty} J_n{}'(ne)\sin 2\pi n(\phi_{\rm Near}-\phi_{\rm p}). \tag{26}$$

Since equations (17) and (18) should be satisfied at the nearest point, we define two discriminants

$$D_1(\varpi) := \cos(f_{\rm Near}+\varpi) + e\cos\varpi \tag{27}$$

$$D_2(\varpi) := \sin(f_{\rm Near}+\varpi) - \sqrt{1-e^2\cos^2\varpi} \tag{28}$$

and search for $\varpi^{(0)}$ satisfying both of $D_1(\varpi^{(0)}) = 0$ and $D_2(\varpi^{(0)}) = 0$ (Fig. 6). Corresponding to the presence of two possible solutions of $\phi_{\rm p}$, there are two solutions of ϖ, which are explementary angles (see Fig. 7).

It should be noted here that both $\phi_{\rm p}$ and ϖ are determined as functions of e. Their dependence on e for a given set of $\tau_{\rm F}$ and $\tau_{\rm N}$ is shown in Fig. 8.

2.4.5 *Initial guess for $a_1 \sin i$*

Once e and ϖ are determined, the projected semimajor axis, $a_1 \sin i$, is determined in units of light travel time, with the help of $\tau_{\max} - \tau_{\min}$, by

$$\frac{a_1 \sin i}{c} = \frac{(\tau_{\max}-\tau_{\min})}{2}\left(1-e^2\cos^2\varpi\right)^{-1/2}. \tag{29}$$

Note that the two solutions of ϖ obtained above lead to an identical value of $a_1 \sin i/c$.

2.4.6 *TD curve for initial guesses*

Substitution of the initial guesses thus obtained into equation (6) leads to an initial guess for the TD curve. Among the two possible pairs of solutions, one of them generates a reasonable TD curve that fits the observations, while the other generates a TD curve that is an almost mirror image of the observed TD curve. The χ^2 value easily discriminates between the two values of ϖ, so this can be automated. Fig. 9 demonstrates the situation, using the initial guesses for the orbital parameters tabulated in Table 2. One of the solutions, with periapsis at the far side, fits the data well, while the other one having periapsis at the near side has a larger value of χ^2/N, so the latter is rejected. Of course, the correct solution is consistent with qualitative expectations described in Section 1; the periapsis of the star is at the near side of the orbit, and the pulsating star passes the periapsis after reaching the nearest point to us, that is, $\pi/2 < \varpi < \pi$.

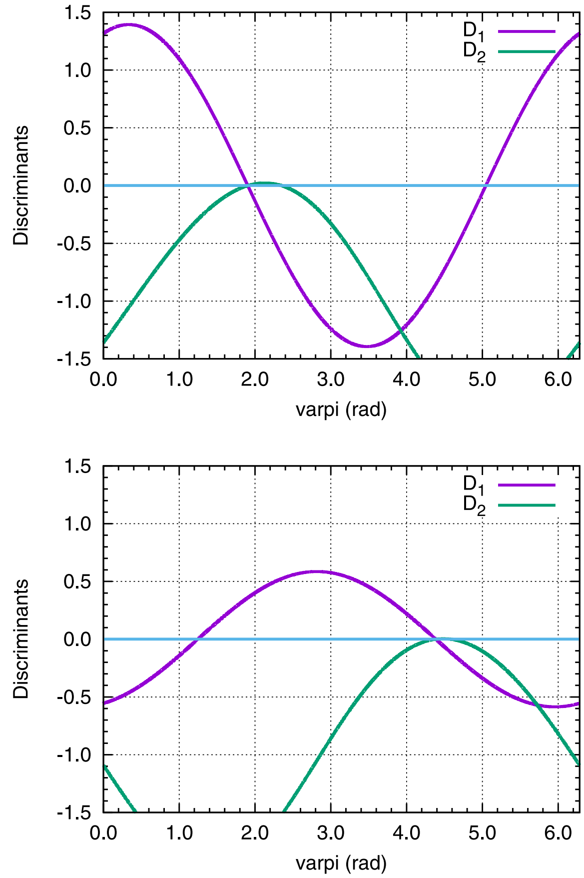

Figure 6. Discriminants from equations (27) and (28) for ϖ of KIC 9651065. The value of ϖ satisfying both of $D_1(\varpi) = 0$ and $D_2(\varpi) = 0$ can be the solution. The upper panel is the case (A) that the periapsis in the near side to us, while the lower panel indicates the case (B) that the periapsis in the far side from us. It is clearly seen that the angle ϖ of the case (A) and that of the case (B) are explementary angles.

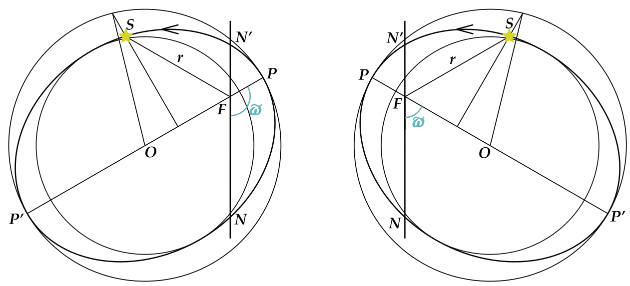

Figure 7. Two solutions satisfying $D_1(\varpi) = D_2(\varpi) = 0$. The line of sight is assumed to be perpendicular to NN' and the star is viewed from the right-hand side. The left-hand panel is the case (A) that the periapsis in the near side to us, while the right-hand panel indicates the case (B) that the periapsis in the far side from us. It is clearly seen that the solution of the case (A) and that of the case (B) are explementary angles.

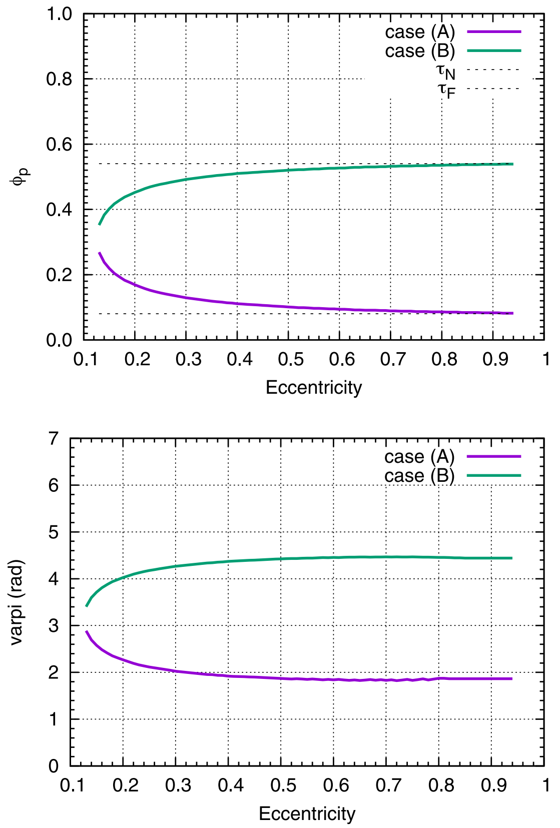

Figure 8. The dependence of $\phi_{\rm p}$ (top panel) and ϖ (bottom panel) on e for a given set of $\tau_{\rm F}$ and $\tau_{\rm N}$ of KIC 9651065. In this case, for $e \lesssim 0.13$, there is no solution satisfying $\Psi(\phi_{\rm p}) = 0$. It is clearly seen that ϖ of the case (A) and that of the case (B) are explementary angles.

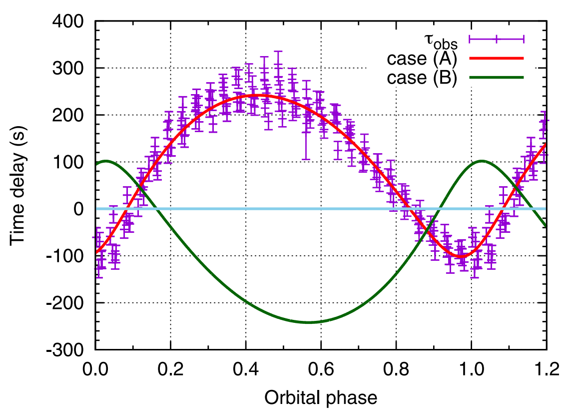

Figure 9. The TD curves for KIC 9651065 constructed with the two sets of initial guesses for the orbital parameters. The red curve, generated with the parameters in the first line of Table 2, matches the observed 'TD' $\tau_{\rm obs}$ (violet dots with error bars), wrapped with the orbital period. On the other hand, the green curve generated with the parameters in the second line of Table 2 has a larger value of χ^2/N, so it is rejected. The periapsis passage $\phi_{\rm p}$ was chosen as the orbital phase of zero. The data points $\tau_{\rm obs}$ were shifted vertically by the amount λ so that they match the red curve.

Fig. 9 demonstrates how well the TD curve computed from the initial guesses reproduces the observed TDs. The orbital phase of zero is chosen so that $\phi_{\rm p} = 0$. The data points of $\tau_{\rm obs}$ were vertically shifted by the amount λ defined by equation (3), so that they match $\tau_{\rm th}$.

Table 2. Possible solutions as initial guesses for the orbital parameters of KIC 9651065 deduced from the observational constraints listed in Table 1. The parameters $\phi_{\rm p}$ and ϖ given in the first line of each are appropriate to be initial guesses, while those in the second line are unsuitable.

Quantity	Value	Units
$\nu_{\rm orb}$	0.003 685 $\pm$ 0.000 011	d^{-1}
$(a_1 \sin i)/c$	174 $\pm$ 25	s
e	0.427 $\pm$ 0.037	
$\phi_{\rm p}$	0.11 $\pm$ 0.04	
	0.51	
ϖ	1.90 $\pm$ 0.23	rad
	4.39	

2.5 Search for the best-fitting parameters

Once a set of initial guesses for $a_1 \sin i$, e, $\phi_{\rm p}$ and ϖ are obtained, we may search for the best-fitting values of these parameters that minimize χ^2/N by iteration. We regard Ω as a fixed value, because the orbital period is already well determined from the Fourier transform of the TD curve. The best-fitting values of the orbital parameters are summarized in Table 3, and the TD curve obtained thusly, matching best the observed TD according to the χ^2 minimization illustrated in Fig. 10, is shown in Fig. 11.

The bottom line of Table 3 lists the mass function $f(m_1, m_2, \sin i)$, defined by

$$f(m_1, m_2, \sin i) := \frac{(m_2 \sin i)^3}{(m_1 + m_2)^2} = \frac{(2\pi)^2 c^3}{G} \nu_{\rm orb}^2 \left(\frac{a_1 \sin i}{c}\right)^3, \tag{30}$$

where m_1 and m_2 denote the masses of the primary (the pulsating star in the present case) and the secondary stars, respectively, and

Table 3. The best-fitting orbital parameters of KIC 9651065 deduced from the observational constraints listed in Table 1.

Quantity	Value	Units
$\nu_{\rm orb}$	0.003 684 $\pm$ 0.000 011	d^{-1}
$(a_1 \sin i)/c$	183.2 $\pm$ 5.0	s
e	0.44 $\pm$ 0.02	
$\phi_{\rm p}$	0.14 $\pm$ 0.02	
ϖ	2.11 $\pm$ 0.05	rad
$f(m_1, m_2, \sin i)$	0.0896 $\pm$ 0.0074	$M_\odot$

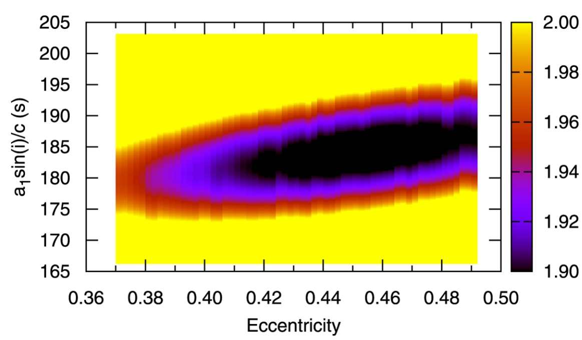

Figure 10. χ^2/N as a function of $(e, a_1 \sin i/c)$ for KIC 9651065.

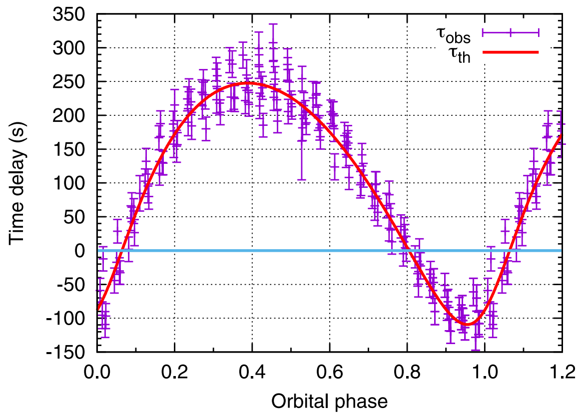

Figure 11. The best-fitting TD curve for KIC 9651065. The periapsis passage ϕ_p was chosen as the orbital phase of zero.

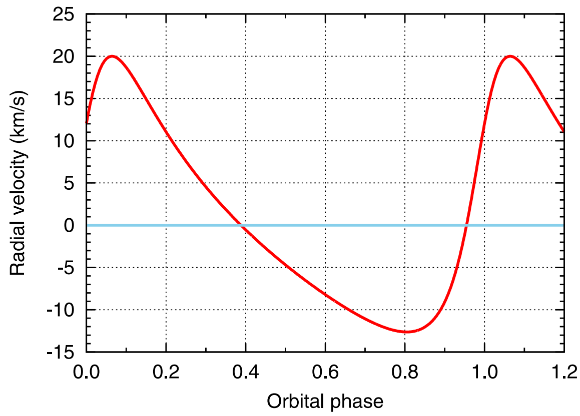

Figure 12. RV of KIC 9651065. The periapsis passage ϕ_p was chosen as the orbital phase of zero.

G is the gravitational constant. The value of $f(m_1, m_2, \sin i)$ gives a minimum secondary mass of $m_2 = 0.82^{+0.04}_{-0.06}\,\mathrm{M}_\odot$ based on an assumption of $m_1 = 1.7\,\mathrm{M}_\odot$, so the secondary is probably a main-sequence G star.

2.6 Uncertainties

The uncertainties on the final orbital parameters are the result of propagation of the observational uncertainties, which are obtained as follows. The uncertainty on the orbital frequency is obtained from a non-linear least-squares fit to the TD curve before phase-folding.

As for $a_1 \sin i/c$ and e, first, we take a2D slice cut of χ^2 in an (e, $a_1 \sin i/c$)-plane (Fig. 10). Then by taking a 1D cut of the plane at the values corresponding to the best-fitting value of $a_1 \sin i/c$, we get a histogram of χ^2 along that line. Since the distribution about that line is approximately Gaussian, the FWHM (full width at half-maximum) of that Gaussian gives the uncertainty. The uncertainty thus evaluated on $a_1 \sin i/c$ for KIC 9651065 is ∼5 s, and that on e is 0.02. The uncertainties on the other parameters are evaluated in the same manner, and they are listed in Table 3.

2.7 Radial velocity

Since $v_{\rm rad} = c\,\mathrm{d}\tau/\mathrm{d}t$, once the orbital parameters are deduced, it is straightforward to obtain the RV:

$$v_{\rm rad} = -\frac{\Omega a_1 \sin i}{\sqrt{1-e^2}}\left[\cos(f+\varpi) + e\cos\varpi\right]. \qquad (31)$$

Fig. 12 shows the RV curve thus obtained for KIC 9651065.

In Murphy et al. (2014), we wrote ‘ RV curves derived with the PM method could be used as input for codes that model eccentric binaries, such as PHOEBE. Given that such codes aim to infer the geometry of the orbit, modelling the TDs themselves might be preferred over the RV curve, since the former give the binary geometry directly and more precisely.’ Our hopes were realized in this work. The RV curve is now provided only as a visualization, it is not required for the derivation of the orbital parameters.

3 EXAMPLE 2: KIC 10990452

Our method is also applicable to pulsators in binary systems with short TDs. In this section, we demonstrate KIC 10990452, for which the range of variation in TD is about 1/4 of the case of KIC 9651065. Fig. 13 shows the TD curve for KIC 10990452. Deviation from a sinusoid indicates that the orbit is eccentric as in the case of Example 1: KIC 9651065. However, contrary to the case of KIC 9651605, its maxima are sharp and the minima are rounded. These facts indicate that periapsis is at the far side of the orbit. Fast fall and slow rise reveal that the star passes the periapsis after reaching the farthest point from us. Table 4 summarizes the observational constraints for KIC 10990452.

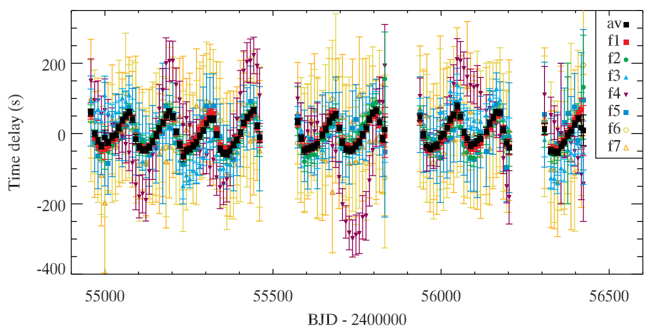

Figure 13. TD curve of KIC 10990452 obtained from seven different pulsation modes. The weighted average is shown as filled black squares.

Table 4. Observational constraints for KIC 10990452.

Quantity	Value	Units
$\tau_{\rm max}$	63.2 ± 12.6	s
$\tau_{\rm min}$	− 45.4 ± 10.0	s
$\nu_{\rm orb}$	0.008 1855 ± 0.0000 142	d^{-1}
A_1	49.22 ± 1.95	s
A_2	13.14 ± 1.32	s
$\phi(\tau_{\rm max})$	0.77 ± 0.02	
$\phi(\tau_{\rm min})$	0.15 ± 0.02	

Substitution of these parameters into equation (23) leads to two roots of $\Psi(\phi_p) = 0$, as shown in Fig. 14, and each solution has ϖ satisfying $D_1(\varpi) = D_2(\varpi) = 0$, as demonstrated in Fig. 15, whose sum is 2π. Initial guesses for the eccentricity, e, and the projected semimajor axis, $a_1 \sin i$, are calculated using equations (13) and (29).

Substitution of the initial guesses thus obtained into equation (6) leads to an initial guess for the TD curve. Among the two possible pairs of solutions, the one giving the smaller value of χ^2/N fits the observations, as shown in Fig. 16. The other set with the larger value of χ^2/N is rejected.

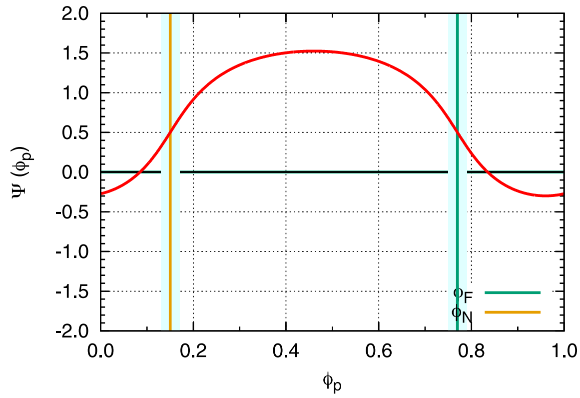

Figure 14. Same as Fig. 5, but for KIC 10990452.

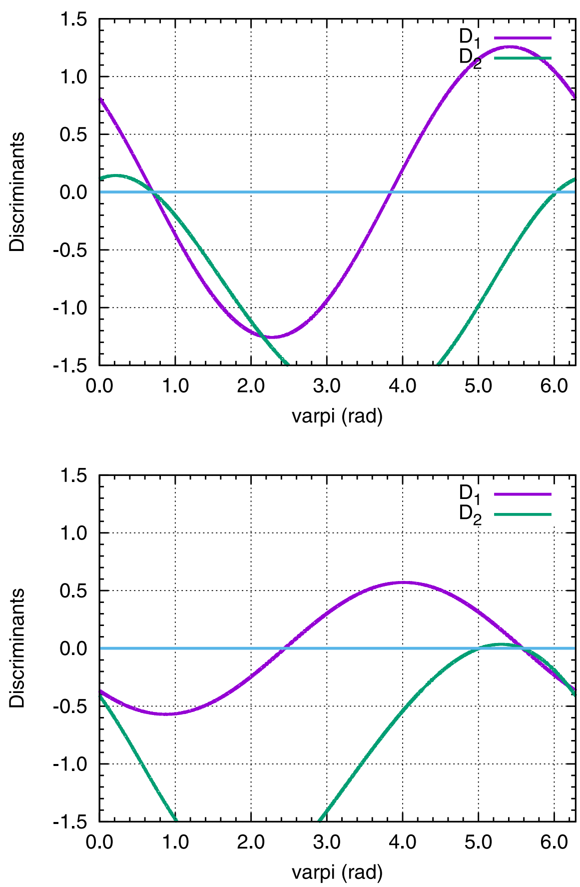

Figure 15. Same as Fig. 6, but for KIC 10990452.

The best-fitting parameters are obtained by searching for the minimum of χ^2/N as a function of $(e, a_1 \sin i)$. Fig. 17 shows a 2D colour map of χ^2/N. The best-fitting parameters are summarized in Table 5, and the TD curve generated with these parameters is shown in Fig. 18. Finally, the RV curve is obtained as shown in Fig. 19.

As seen in the case of KIC 10990452, the present method is applicable without any difficulty to pulsators in binary systems showing TD variations of several tens of seconds. Judging from the error bars in the observed TDs of *Kepler* pulsators, and from the binaries we have found so far, we are confident that the present method is valid for stars showing TD variations exceeding $\sim\pm 20$ s. While it may be possible to find binaries with even smaller TD variations, such cases will be close to the noise level of the data

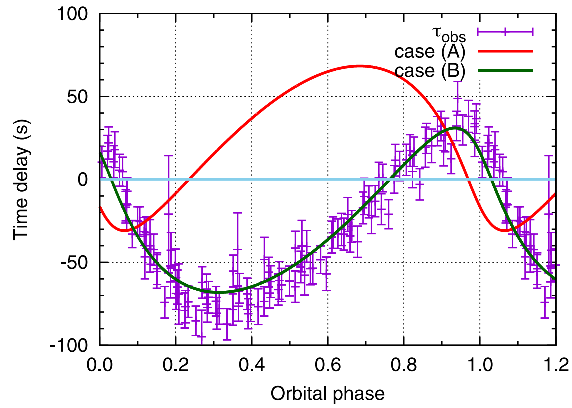

Figure 16. Same as Fig. 9 but for KIC 10990452. The green curve, generated with one of the solutions of parameters giving the smaller value of χ^2/N, where N denotes the number of data points, fits the data well. On the other hand, the red curve generated with the other set of parameters has a larger value, so it is rejected. The periapsis passage $\phi_{\rm p}$ was chosen as the orbital phase of zero.

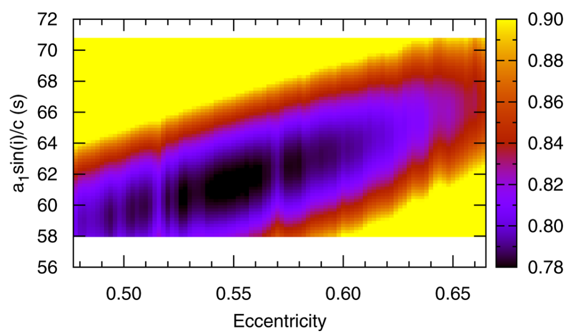

Figure 17. χ^2/N as a function of $(e, a_1 \sin i/c)$ for KIC 10990452.

Table 5. The best-fitting orbital parameters of KIC 10990452.

Quantity	Value	Units
$\nu_{\rm orb}$	$0.008\,190 \pm 0.000\,014$	d^{-1}
$(a_1 \sin i)/c$	61.3 ± 8.0	s
e	0.55 ± 0.03	
$\phi_{\rm p}$	0.89 ± 0.02	
ϖ	5.81 ± 0.05	rad
$f(m_1, m_2, \sin i)$	$0.01\,658 \pm 0.00\,649$	$\mathrm{M}_\odot$

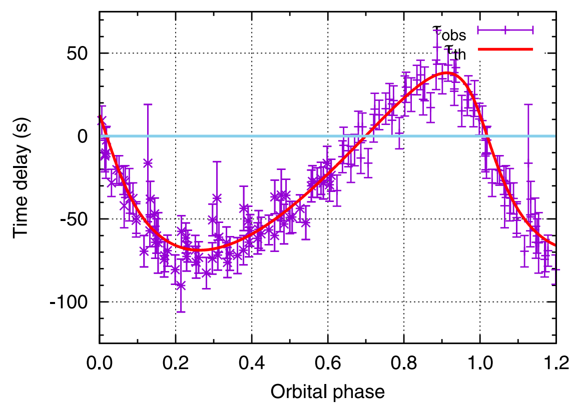

Figure 18. The best-fitting TD curve for KIC 10990452. The periapsis passage $\phi_{\rm p}$ was chosen as the orbital phase of zero.

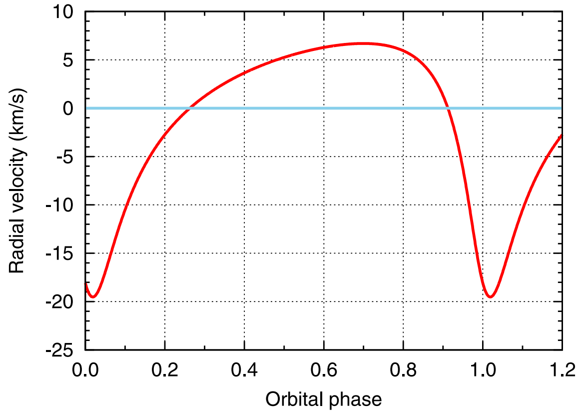

Figure 19. RV of KIC 10990452. The periapsis passage ϕ_p was chosen as the orbital phase of zero.

and may require external confirmation. The noise limit is discussed further in Section 4.

4 EXAMPLE 3: THE MORE ECCENTRIC CASE OF KIC 8264492

Fig. 20 shows the TD curve for another star, KIC 8264492. Deviation from a sinusoid indicates that the orbit is highly eccentric, and the number of harmonics to the orbital period visible in Fig. 21, as well as their high amplitudes, confirm this. Let us see if our method is valid for such a highly eccentric binary system. Its maxima are sharp and the minima are rounded, indicating that periapsis is at the far side of the orbit. Fast fall and slow rise reveal that the star passes the periapsis after reaching the farthest point from us.

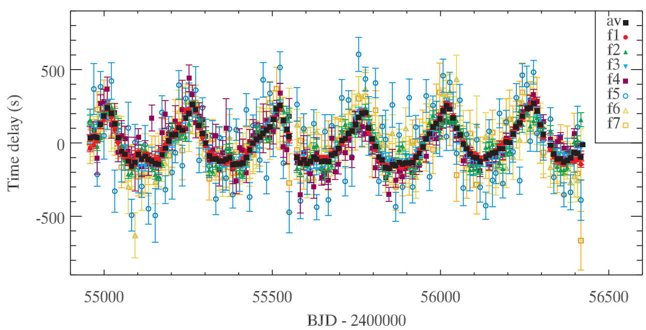

Figure 20. TD curve of KIC 8264492 obtained from seven different pulsation modes. The weighted average is shown as filled black squares.

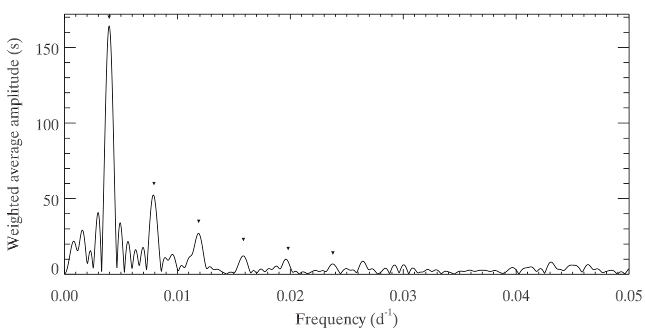

Figure 21. Fourier transform of the TD curve of KIC 8264492 shown in Fig. 20. Exact multiples of the orbital frequency (0.003 94 d^{-1}) are indicated, showing the many harmonics and implying high eccentricity.

Table 6. Observational constraints for KIC 8264492.

Quantity	Value	Units
$\tau_{\rm max}$	214.6 $\pm$ 42.9	s
$\tau_{\rm min}$	$-$ 132.5 $\pm$ 26.5	s
$\nu_{\rm orb}$	0.003 9408 $\pm$ 0.0000 158	d^{-1}
A_1	159.90 $\pm$ 3.61	s
A_2	50.41 $\pm$ 3.61	s
$\phi(\tau_{\rm max})$	0.76 $\pm$ 0.02	
$\phi(\tau_{\rm min})$	0.12 $\pm$ 0.02	

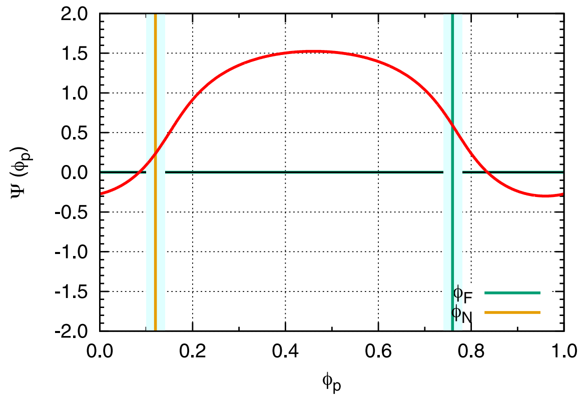

Figure 22. Same as Fig. 5, $\Psi(\phi_p)$ (red curve), but for KIC 8264492.

The orbital frequency, the amplitudes of the highest component and the second one, and the orbital phases at the maximum and the minimum of the TDs are deduced from the Fourier transform. They are summarized in Table 6. Substitution of these parameters into equation (23) enables numerical root-finding of $\Psi(\phi_p) = 0$, as shown in Fig. 22. One root corresponds to the case (A) that the pulsating star in question passes the periapsis soon after the nearest point to us, and the other corresponds to the case (B) that the star passes the apoapsis just before the furthest point from us. Corresponding to the presence of two possible solutions of ϕ_p, there are two solutions of ϖ, which are explementary angles (see Fig. 23).

Substitution of the initial guesses thus obtained into equation (6) leads to an initial guess for the TD curve. As in the case of KIC 9651605, among the two possible pairs of solutions, one of them generates a reasonable TD curve that fits the observations, while the other generates a TD curve that is an almost mirror image of the observed TD curve, with a larger value of χ^2/N (Fig. 24). The correct solution is consistent with qualitative expectations described at the beginning of this subsection; the periapsis of the star is at the far side of the orbit, and the star passes the periapsis after reaching the farthest point from us, that is, $3\pi/2 < \varpi < 2\pi$.

Fig. 24 shows the TD curve, computed for the initial guesses, plotted with the observed TDs. The orbital phase of zero is chosen so that $\phi_p = 0$. The data points of $\tau_{\rm obs}$ were vertically shifted by the amount λ, defined by equation (3), so that they match $\tau_{\rm th}$. Unlike the earlier example of KIC 9651065, there remain systematic residuals in the TD curve for KIC 8264492.

The best-fitting parameter derived from a 2D colour map of χ^2/N (Fig. 25) are summarized in Table 7, and Fig. 26 and Fig. 27 show the TD curve and the RV curve generated with these parameters, respectively. Hence, with KIC8264492, we have demonstrated the validity and utility of the PM method, even for systems with high eccentricity.

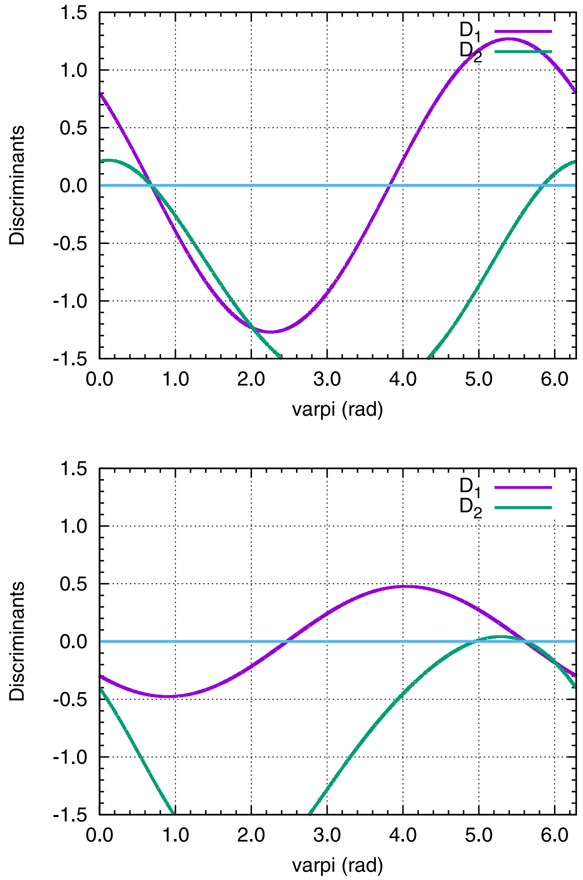

Figure 23. Same as Fig. 6 but for KIC 8264492. The upper panel is the case that the periapsis is in the near side to us, while the lower panel indicates the case that the periapsis is in the far side from us.

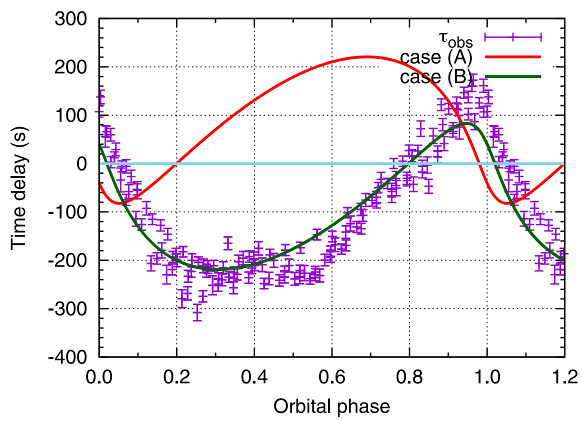

Figure 24. Same as Fig. 9 but for KIC 8264492. The violet curve, generated with the parameters in the first line of Table 6, fits the data well. On the other hand, the red curve generated with the other set of parameters has a larger value of χ^2/N, so it is rejected. The periapsis passage ϕ_p was chosen as the orbital phase of zero.

5 DISCUSSION

In this work, we have primarily focussed on deriving full orbital solutions for highly eccentric binaries. Our first example, KIC 9651065, was also studied in our previous work (Murphy et al. 2014), and so a direct evaluation of the improvement in technique is possible.

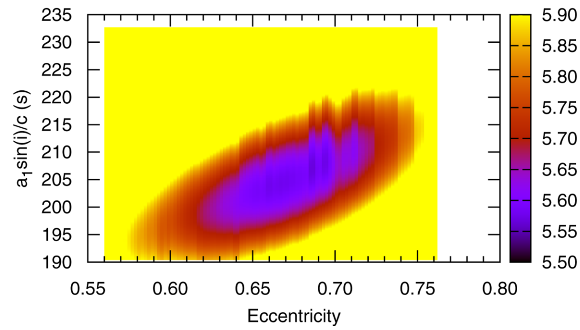

Figure 25. χ^2/N as a function of $(e, a_1 \sin i/c)$ for KIC 8264492.

Table 7. The best-fitting orbital parameters of KIC 8264492 deduced from the observational constraints listed in Table 6.

Quantity	Value	Units
$\nu_{\rm orb}$	$0.003\,940 \pm 0.000\,016$	d^{-1}
$(a_1 \sin i)/c$	204.8 ± 25.8	s
e	0.67 ± 0.04	
$\phi_{\rm p}$	0.80 ± 0.02	
ϖ	5.28 ± 0.05	rad
$f(m_1, m_2, \sin i)$	$0.143\,08 \pm 0.05\,410$	$\mathrm{M}_\odot$

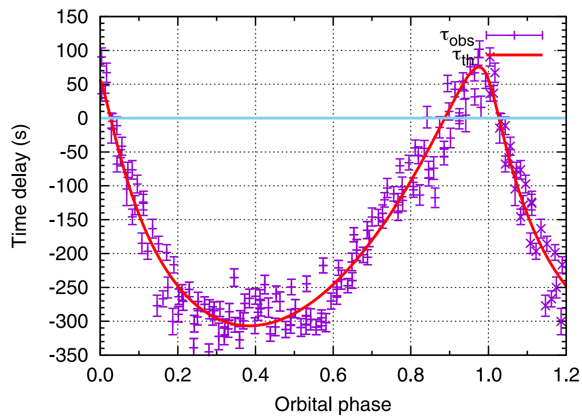

Figure 26. The best-fitting TD curve for KIC 8264492. The periapsis passage $\phi_{\rm p}$ was chosen as the orbital phase of zero.

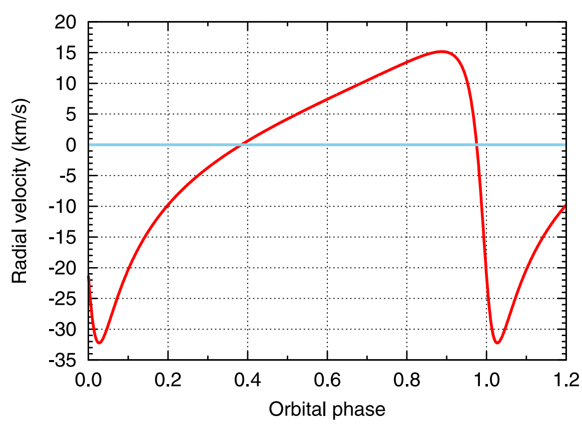

Figure 27. Same as Fig. 12 but for KIC 8264492.

Table 8. Comparison of the uncertainties in the orbital parameters for KIC 9651065. (i) Those calculated here by fitting the TD data in this work versus (ii) those calculated through fitting RVs obtained by taking pairwise differences of the TD data in previous work.

Quantity	Units	Value This work	Value Previous work
$\nu_{\rm orb}$	d^{-1}	$0.003\,684 \pm 0.000\,011$	$0.003\,667 \pm 0.000\,016$
$(a_1 \sin i)/c$	s	183.2 ± 5.0	185.0 ± 10.0
e		0.44 ± 0.02	0.47 ± 0.03
ϖ	rad	2.11 ± 0.05	2.01 ± 0.30
$f(m_1, m_2, \sin i)$	$M_\odot$	0.0896 ± 0.0074	0.0916 ± 0.0108
χ^2/N		1.80	2.21

5.1 Improvement in technique

The improvement can be seen in two ways. Firstly, the quality of the fit of the theoretical TD curve to the data can be evaluated in terms of the reduced χ^2 parameter. The former method gave a value of 2.21 for KIC 9651065, compared to 1.80 for the analytical approach presented in this work. Secondly, one can compare the uncertainties in the orbital parameters obtained by each method. Table 8 shows that smaller uncertainties, particularly in ϖ, result from fitting the TDs directly, rather than fitting the RVs obtained by pairwise differences of the TD data.

There are also new improvements in the elimination of systematic errors. Previously, the eccentricity would be underestimated due to the reliance on the approximation in equation (13) (equation 5 in Murphy et al. 2014). This was also strongly subject to noise spikes in the Fourier transform of the TDs. Now, that approximation is only used as an initial guess, and the search for the minimum in the χ^2 distribution obtains the best-fitting value more reliably.

5.2 Factors affecting the minimum measurable TD

The detection of the smallest companions, which give rise to the smallest TDs, requires a thorough understanding of the dominant contributors to the noise and how that noise can be mitigated.

There are many ways that the noise level is affected by the properties of the pulsation and/or the sampling. The cadence of the observations has little impact on the quoted 20-s limit because *Kepler* observations were mostly made in a single cadence (long-cadence at 30 min), though for stars with ample short-cadence (60-s) data the phase errors can be reduced by a factor ∼5 (Murphy 2012). The noise can be reduced when the star oscillates in many modes, providing they have similar amplitudes to the highest amplitude mode. The noise in the weighted average TDs is then reduced, though taking the weighted average means that the inclusion of more modes of much lower amplitudes than the strongest mode does not help, since phase uncertainties scale inversely with amplitude. Also for this reason, we do not consider modes with amplitudes below one tenth of that of the strongest mode in each star, and high-amplitude pulsators are clearly more favourable. Furthermore, we consider a maximum of nine modes per star due to diminishing return in computation time. Finally, it is noteworthy that the smallest detectable TD variation has no theoretical dependence on the orbital period, providing the orbit is adequately sampled.

6 CONCLUSIONS

We have developed upon our previous work (Murphy et al. 2014), where we showed how light arrival TDs can be obtained through pulsational phase modulation of binary stars. Formerly, RVs were calculated numerically from the TDs and the orbital parameters were obtained from the RV curve. Here, we have shown how the same orbital parameters are obtainable directly from the TDs. The RV curve is now provided only as a visualization; it is not a necessary step in solving the orbit.

We will be applying this method to the hundreds of classical pulsators for which we have measured TDs with *Kepler* data, with the aim of delivering a catalogue of TD and RV curves alongside orbital parameters in the near future. We likewise encourage developers and users of binary modelling codes to consider taking TDs as inputs.

ACKNOWLEDGEMENTS

We are grateful to the entire *Kepler* team for such exquisite data. We would like to thank Tim Bedding for his suggestions and encouragement to pursue a method that derives orbital parameters through direct fitting of the TDs. We thank the anonymous referee for suggestions that improved this paper.

This research was supported by the Australian Research Council, and by the Japan Society for the Promotion of Science. Funding for the Stellar Astrophysics Centre is provided by the Danish National Research Foundation (grant agreement no. DNRF106). The research is supported by the ASTERISK project (ASTERoseismic Investigations with *SONG* and *Kepler*) funded by the European Research Council (grant agreement no. 267864).

REFERENCES

Balona L. A., 2014, MNRAS, 443, 1946
Brouwer D., Clemence G. M., 1961, Methods of Celestial Mechanics. Academic Press, New York
Buchler J. R., Goupil M.-J., Hansen C. J., 1997, A&A, 321, 159
Freire P. C., Kramer M., Lyne A. G., 2001, MNRAS, 322, 885
Freire P. C., Kramer M., Lyne A. G., 2009, MNRAS, 395, 1775
Koen C., 2014, MNRAS, 444, 1486
Murphy S. J., 2012, MNRAS, 422, 665
Murphy S. J., Shibahashi H., Kurtz D. W., 2013, MNRAS, 430, 2986
Murphy S. J., Bedding T. R., Shibahashi H., Kurtz D. W., Kjeldsen H., 2014, MNRAS, 441, 2515
Shibahashi H., Kurtz D. W., 2012, MNRAS, 422, 738
Shibahashi H., Kurtz D. W., Murphy S. J., 2015, MNRAS, in press

This paper has been typeset from a TEX/LATEX file prepared by the author.